Lattice dynamics and hyperfine interactions in ZnO and ZnSe at high external pressures

H. Karzel, W. Potzel, M. Köfferlein, W. Schiessl, M. Steiner, U. Hiller, and G. M. Kalvius
Physik-Department E15, Technische Universität München, D-85747 Garching, Germany

D. W. Mitchell* and T. P. Das
Department of Physics, State University of New York at Albany, Albany, New York 12222

P. Blaha and K. Schwarz
Institut für Technische Elektrochemie, Technische Universität Wien, A-1060 Vienna, Austria

M. P. Pasternak
School of Physics and Astronomy, Tel Aviv University, 69978 Tel Aviv, Israel
(Received 14 April 1995; revised manuscript received 20 December 1995)

The II-VI semiconductors ZnO and ZnSe have been investigated by x-ray and ^{67}Zn-Mössbauer spectroscopy at high external pressures. In ZnSe, the recoilfree fraction f increases from $f=0.50\%$ at ambient pressure to 1.19% at 6.1 GPa. It then decreases to $f=0.92\%$ as the pressure is further raised to 8.2 GPa. This decrease of f is caused by softening of phonon modes which occurs far below the crystallographic phase transition (13.5 GPa). In the high-pressure phase of ZnO (NaCl structure), low-frequency acoustic-phonon modes become harder and high-frequency optic modes become softer as compared to ZnO (wurtzite structure). Modern theoretical Hartree-Fock cluster and full potential scalar-relativistic linearized-augmented plane-wave calculations have been performed. These calculations reveal that in both systems covalent contributions to the chemical bond determine the change of the s electron density $\rho(0)$ at the Zn nucleus between the different crystallographic phases as well as the electric-field-gradient tensor in ZnO (wurtzite). In particular, $\rho(0)$ in ZnO (NaCl phase) is reduced compared to $\rho(0)$ in ZnO (wurtzite phase) by $-1.15e/a_0^3$. Thus, contrary to observation for ZnSe, the electrical conductivity in ZnO (NaCl phase) is *not* expected to increase in comparison with the low-pressure wurtzite structure.

I. INTRODUCTION

The sp-bonded binary compounds of the groups II and VI of the Periodic Table have been at the center of semiconductor research during recent years. In particular, the application of II-VI semiconductors in optical devices has reached a high experimental level. For example, ZnSe is ideally suited[1] for fabrication of blue-light emitting diodes and quantum-well devices. But the final realization of those features in technical applications is still curtailed by the lack of some important fundamental information pertaining to these materials. It requires further elucidation and deeper knowledge of the electronic and lattice properties. It is the purpose of this work to provide further understanding of these semiconductors by probing some of their properties under high pressure.

At ambient pressure most of the chalcogenides crystallize in either the hexagonal wurtzite or the cubic zinc-blende structure or both. Common to all structures is the tetrahedral coordination of Zn by four anions and vice versa, in a sp^3 covalent bonding. At high pressures ZnO, ZnS, ZnSe, and possibly ZnTe, undergo a crystallographic phase transition into the sixfold-coordinated NaCl structure.[2–4] This is accompanied by pronounced changes in their electronic features such as a drastic increase in the electrical conductivity σ.[2] The mechanism responsible for this latter phenomenon where σ increases by seven orders of magnitude has been clarified for ZnSe only lately. On the basis of earlier optical measurements in ZnS,[5,6] it was suggested that this large increase in σ is due to high concentration of defects. Recent dc-conductivity studies in ZnSe,[7] however, show that a semiconductor-metal transition occurs. The same ambiguity still exists for the case of ZnTe. No high-pressure conductivity measurements were carried out in ZnO.

Structural properties and questions concerning crystal stability, in particular transition pressures, have been discussed within several semiempirical models.[8–12] In addition, more recently a number of theoretical *ab initio* calculations has become available with emphasis on crystallographic phase transitions[13,14] as well as on electronic structure concerned with hyperfine interactions in the solid state.[15–18] However, experimental microscopic data on electronic structure at high pressures are scarce. A unique probe for hyperfine interaction measurements is ^{67}Zn-Mössbauer spectroscopy, a method extremely sensitive to changes in the s electron density,[16,19] therefore to the valence state of Zn, and to lattice dynamics via the recoil free fraction f (Lamb-Mössbauer factor).

In this paper we report on experimental and theoretical investigations of ZnO and ZnSe at high external pressures. We describe results obtained from high-pressure Mössbauer spectroscopy and x-ray diffraction. To reach deeper insight into the electronic structure of both compounds we have performed *ab initio* Hartree-Fock (HF) cluster as well as scalar-relativistic linearized-augmented plane-wave (LAPW) calculations. In addition for ZnSe, we combine our ^{67}Zn-Mössbauer study with lattice-dynamic calculations us-

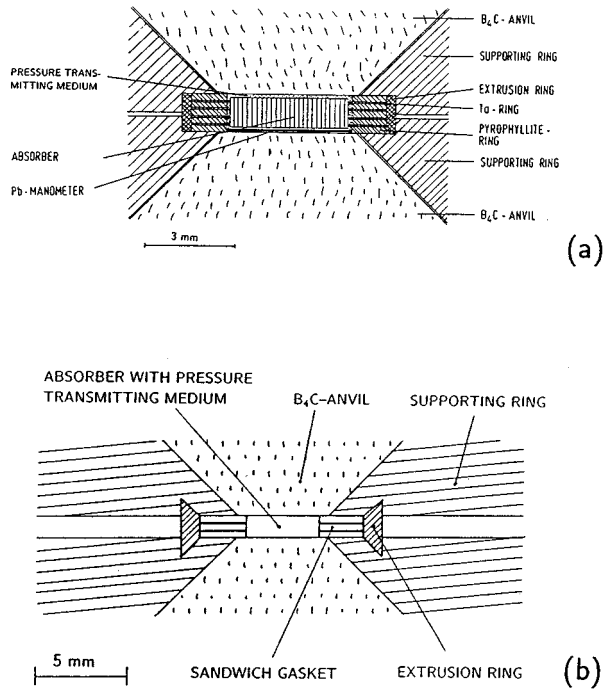

FIG. 1. Two types of sandwich gaskets, (a) type I, (b) type II, used in the high-pressure cells for Mössbauer experiments.

ing an 11-parameter rigid-ion model to reveal the softening of phonon modes preceding the crystallographic phase transition.

II. EXPERIMENTAL DETAILS

A. Mössbauer spectrometer for high pressures

The high-pressure, low-temperature Mössbauer spectrometer for the 93.31-keV resonance in ^{67}Zn is based on designs described earlier.[20,21] The pressure is applied to the absorber (^{67}ZnO powder or ^{67}ZnSe powder) by two symmetrical anvils made from sintered B_4C inside a CuBe high-pressure clamp. The dimensions of the absorber are large, 4 mm in diameter and 2 mm in height, to ensure satisfying count rates in the 93.31-keV window. The enrichment in ^{67}Zn was $\approx$90% for ^{67}ZnO and ^{67}ZnSe with corresponding absorber thicknesses of 590 mg/cm^2 (ZnO) and 300 mg/cm^2 (ZnSe) of ^{67}Zn, respectively. For the highest pressure on ZnO the height was reduced to 1.2 mm, the corresponding absorber thickness was only 310 mg/cm^2 of ^{67}Zn. Quasihydrostatic conditions were obtained by adding a mixture of methanol ethanol in the ratio 4:1.[22] The relatively large dimensions of the absorber required the use of sandwich gaskets.[21] We have employed two different types which are shown in Fig. 1. The main feature of both types is a sandwich gasket of pyrophyllite and tantalum disks acting also as a collimator for the 93.31-keV γ radiation. For the ZnO and ZnSe absorbers with 2 mm in height we used five pyrophyllite and four tantalum disks [Fig. 1(a)], for the ZnO absorber of 1.2 mm the corresponding numbers were three and two, respectively [Fig. 1(b)]. The main advantages of type I [Fig. 1(a)] are the large amount of absorber material and the fact that the gasket is well embedded into the supporting rings and highly stable despite the large sample volume. The main disadvantage, however, is the rather small separation between the upper and lower supporting rings. As a consequence, the volume reduction of sample and gasket can only be relatively small when pressure is applied and will reach a limit when finally both supporting rings are in close contact. Thus, care has to be taken that the powder sample is well prepressed before starting the actual high-pressure experiment. In addition, with the zinc chalcogenides we found a drastic volume collapse of typically 15% at the crystallographic phase transition (see Sec. III). This made it impossible to use gasket type I for pressures above 9 GPa. Gasket type II [Fig. 1(b)] remedies these problems. Here the main disadvantages are the smaller absorber thickness, the less effective collimation of the 93.31-keV γ rays, and a reduced stability of the gasket with essentially only the extrusion ring being embedded in the supporting rings. In particular, the rather small absorber thickness prevented us from investigating the phase transition in ZnSe by ^{67}Zn-Mössbauer spectroscopy (see Sec. IV). As described in more detail in Refs. 20 and 21, the pressure is applied to the sample at room temperature by means of a hydraulic press. Thereafter the clamp is cooled to cryogenic temperatures to perform the Mössbauer experiments. The force is stored in five steel springs inside the clamp. The springs also compensate for the differences in thermal expansion between the clamp and the components of the high-pressure cell when cooling to cryogenic temperatures. For pressure changes the device has to be warmed up to room temperature. In all our ^{67}Zn-Mössbauer experiments the pressure at the absorber was determined *in situ* at cryogenic temperatures by a lead strip acting as a pressure gauge.[23,24] This lead manometer is indicated in Fig. 1(a), only. Despite the large dimensions of the samples, the pressure gradients across the samples as estimated from the superconducting transitions of the lead manometer were smaller than 10% at a pressure of $\approx$10 GPa.

A piezoelectric quartz drive which moves the source, is mounted directly on top of the pressure clamp to avoid unwanted vibrational motions between source and absorber which would cause spectral distortions. The whole system is cooled to liquid-helium temperatures in a metal cryostat to perform the ^{67}Zn-Mössbauer experiments. Doppler velocities were calibrated using the known quadrupole interactions in ^{67}ZnO (Ref. 25) and ^{67}Zn metal[26] at ambient pressure and liquid-helium temperature. Further details on the spectrometer are given in Refs. 19–21.

As Mössbauer sources we employed ^{67}GaZnO single crystals. They were squares of 6 mm$\times$6 mm and of 1 mm thickness, the c axis being perpendicular to the faces. The ^{67}Ga (half-life of $T_{1/2}$=78 h) activity was produced *in situ* by 28-MeV proton bombardment at the cyclotron KAZ of the Forschungszentrum Karlsruhe. After annealing the crystals at 700 °,[25] they were used in our spectrometer with the c axis being parallel to $\mathbf{k}_\gamma$, the direction of observation of the γ rays.

The γ rays were detected by an intrinsic Ge diode of 10 mm thickness and 40 mm diameter coupled to fast nuclear pulse amplifiers.[27] Typical signal-to-background ratios of $S/(S+B)\approx 0.75$ were obtained at count rates up to 110 000 s^{-1} in the 93.31-keV window. The data pulses were col-

lected in time mode into a 1024-channel analyzer whose channel advance rate was synchronized to the drive frequency (typical 400 Hz) by a phase-locked-loop circuit.[28]

B. X-ray diffractometer for high pressures and low temperatures

We used an angular dispersive x-ray diffractometer of the Guinier type which includes a liquid-helium cryostat.[29,30] Due to the small sample size, high-pressure cells with B_4C anvils are sufficient up to pressures of ≈ 13 GPa. The design is very similar to that of the cells for the Mössbauer measurements described above, except for the pressure determination. In addition to ZnO or ZnSe powder the sample volume also contained a thin layer of NaCl or CsCl powder separated from the zinc compounds by scotch tape. To derive the pressure at a particular temperature we determined the lattice constants from the angular reflections and used the known equations of state of NaCl (Ref. 31) or CsCl.[32]

For pressures above 13 GPa we employed a diamond-anvil cell as described in more detail in Ref. 33. Pressure determination was accomplished by the ruby fluorescence method in connection with the calibration of the ruby lines given in Ref. 34.

To ensure sufficient transmission through the anvils we used $K\alpha_1$ x rays of Mo. They were detected by a position sensitive proportional counter. For further details see Refs. 29 and 30.

III. RESULTS

A. X-ray-diffraction measurements

Figure 2 displays the pressure dependence of the unit-cell volume for ZnSe and ZnO at room temperature. At ambient pressure ZnSe and ZnO crystallize in cubic zinc-blende (sphalerite) and hcp (wurtzite) structure, respectively. Both compounds exhibit a crystallographic phase transition to the NaCl structure at high pressures. This phase change in ZnO has been observed without adding material stabilizing the rocksalt structure.[3,35] The solid lines in Fig. 2 represent least-squares fits using the Birch-Murnaghan equation.[37] Table I summarizes our results for the lattice constants, transition pressures, bulk moduli, and volume changes when extrapolating the NaCl phase to ambient pressure. Results on ZnS (Ref. 5) are also included. The phase transition in ZnTe at ≈ 9.5 GPa is more complex[36] and will not be considered further in this paper. The hysteresis of the transition is very pronounced in all three systems as can be seen from the large differences of transition pressures with increasing ($P_T^{\uparrow}$) and decreasing ($P_T^{\downarrow}$) pressure. The volume change at the transition is typically 15%. The bulk moduli B_0 are considerably enhanced in the NaCl structure as compared to the ambient pressure phase. At the transition pressures indicated by the vertical lines ($P_T^{\uparrow}, P_T^{\downarrow}$) in Fig. 2 half of the material (as determined from the corresponding x-ray patterns) has accomplished the phase transition. In two cases (ZnSe at ≈ 13 GPa and ZnO at ≈ 2 GPa) the coexistence of both structures could be followed over a rather extended pressure range.

For ZnSe we performed, in addition, x-ray measurements at 8.8 GPa and at temperatures of 79.8 and 13.5 K. No crystallographic transition was observed yet under these conditions (see Sec. IV A).

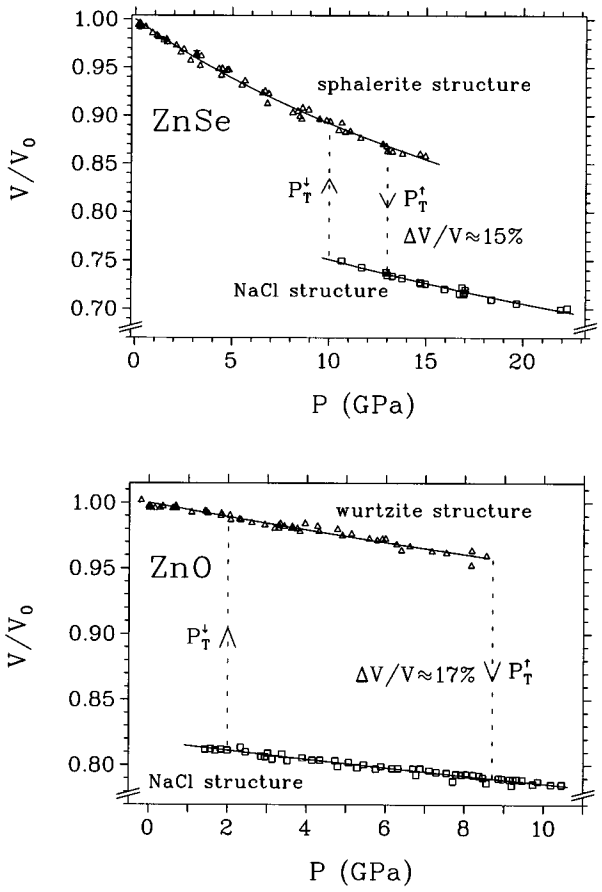

FIG. 2. Pressure dependence of the unit-cell volume for ZnSe and ZnO at room temperature. The solid lines represent fits to the Birch-Murnaghan equation. The arrows indicate the large hysteresis of the transition when increasing and releasing pressure. At the transition pressure ($P_T^{\uparrow}, P_T^{\downarrow}$) half of the material has accomplished phase transition.

B. Mössbauer measurements

1. ZnSe

Figure 3 displays Mössbauer absorption spectra recorded at 4.2 K and three different pressures. The doublet with intensity ratio of 2:1 reflects the splitting in the ^{67}GaZnO source (see Sec. II A). Due to its (cubic) zinc-blende structure, ZnSe exhibits a single absorption line only. The separation of the doublet and the intensity ratio were fixed to their well-known values (4.785 μm/s and 2:1, respectively) of a ^{67}GaZnO source.[25] For the least-squares fits shown in Fig. 3, we have chosen as free parameters the position of the line with larger intensity, the total absorption area A beneath the Lorentzian doublet, a common linewidth Γ (full width at half maximum, FWHM), and the transmission far outside the resonance. Table II lists the results of the fits.

Although the statistical errors in the spectra are relatively large, the base line at large velocities, the area, and the position can be determined reasonably well. The area increases at first with pressure, but decreases again at 8.2 GPa. The position of the absorption doublet increases only slightly from 61.14(8) μm/s at ambient pressure to 63.6(5) μm/s at 8.2 GPa. All changes with pressure are completely revers-

TABLE I. Results for the structural parameters of ZnO and ZnSe. Results for ZnS from Ref. 5 are also included. Values listed for the lattice constants, bulk moduli, and volume changes of the high-pressure phase were obtained by extrapolating to ambient pressure. The volumina V_0 are given per formula unit. The value for B_0' was fixed to 4.0 for all compounds. $P_T^{\uparrow}$ and $P_T^{\downarrow}$ are the transition pressures when increasing ($\uparrow$) and decreasing ($\downarrow$) pressure.

	ZnO	ZnS	ZnSe
Structure	Wurtzite	Sphalerite	Sphalerite
a_0 (Å)	3.2496(6)	5.413(13)	5.667(4)
c_0 (Å)	5.2042(20)		
V_0 (Å^3)	23.796(11)	39.65(30)	45.504(32)
B_0 (GPa)	183(7)	75.0(2.0)	69.3(1.1)
B_0'	4 (fix)	4 (fix)	4 (fix)
	High-pressure phase (index H):		
Structure	NaCl	NaCl	NaCl
a_0 (Å)	4.271(2)	5.060(15)	5.292(12)
V_{0H} (Å^3)	19.484(11)	32.38(30)	37.050(22)
B_{0H} (GPa)	228(7)	104(6)	104(6)
B_{0H}'	4 (fix)	4 (fix)	4 (fix)
$1-V_{0H}/V_0$	0.1813(10)	0.183(10)	0.186(5)
	Parameters at the transition pressure $P_T^{\uparrow}$ when increasing pressure:		
$P_T^{\uparrow}$ (GPa)	8.7(5)	14.7(7)	13.0(5)
$V(P_T^{\uparrow})/V_0$	0.957(3)	0.864	0.868(4)
$V_H(P_T^{\uparrow})/V_{0H}$	0.965(2)	0.893	0.903(5)
$1-V_H(P_T^{\uparrow})/V(P_T^{\uparrow})$	0.175(3)	0.156	0.153(6)
$P\uparrow\cdot[V(P_T^{\uparrow})-V_H(P_T^{\uparrow})]$ (eV)	0.22(1)	0.49	0.49(3)
	Parameters at the transition pressure $P_T^{\downarrow}$ when decreasing pressure:		
$P_T^{\downarrow}$ (GPa)	2.0(5)	≈ 10	9.5(5)
$V(P_T^{\downarrow})/V_0$	0.989(3)	0.898	0.896(5)
$V_H(P_T^{\downarrow})/V_{0H}$	0.991(2)	0.921	0.925(5)
$1-V_H(P_T^{\downarrow})/V(P_T^{\downarrow})$	0.180(3)	0.162	0.159(7)
$P_{\downarrow}\cdot[V(P_T^{\downarrow})-V_H(P_T^{\downarrow})]$ (eV)	0.053(13)	0.36	0.39(3)

ible. The pressure of transition to the NaCl phase ($p=13.5$ GPa) in ZnSe could only be reached in x-ray measurements. Due to technical limitations we could only attain 8.2 GPa in our Mössbauer high-pressure cell.

2. ZnO

Figure 4 shows Mössbauer absorption spectra obtained at 4.2 K and four different pressures. The five-line patterns at 0 and 1.2 GPa reflect the quadrupole interaction in the hcp (wurtzite) source (doublet with intensity ratio of 2:1, see Secs. II A and III B 1) and in the ZnO powder absorber (also wurtzite structure), the latter giving rise to three transitions.[25] The broken lines in the spectrum at ambient pressure (Fig. 4, top) indicate the superposition of three source doublets resulting in a five-line pattern with relative intensities of 1:2:1:3:2 in the order of increasing Doppler velocities. The spectrum at 1.2 GPa shows considerable additional line-broadening and a drastic increase of the asymmetry parameter of the electric-field-gradient tensor (see Sec. IV). The spectrum labeled 4.4 GPa was recorded after first increasing pressure to 7.8 GPa and then releasing it to 4.4 GPa. We observe a superposition of two quite different patterns: the first one which is centered at $S_C\approx 0$ μm/s is similar to the spectrum recorded at 1.2 GPa. The second pattern which has a center shift $S_C\approx -21$ μm/s exhibits a broad unresolved absorption dip together with a sharper doublet also centered at $S_C\approx -21$ μm/s. At still higher pressures (9.0 GPa, Fig. 4 bottom) only the second pattern remains, which according to our x-ray data (see Sec. III A) has to be attributed to ZnO in the NaCl structure. The spectrum labeled 4.4 GPa indicates a partial transformation of ZnO from the hcp (wurtzite) to the cubic (NaCl) structure.

All spectra of Fig. 4 exhibit line broadening. The data are better described by Gaussian than by Lorentzian line profiles. The five-line patterns were fitted by a superposition of three Gaussian doublets (see Fig. 4, top). Table III summarizes the results for ZnO (wurtzite structure) and also lists the values for S_C, the quadrupole coupling frequency $f_Q=eQV_{zz}/h$, and the asymmetry parameter η of the electric- field-gradient (EFG) tensor.

The large hysteresis of the phase transition first seen in the x-ray measurements was fully corroborated by the Mössbauer experiments. For example, the spectrum at 4.4 GPa in Fig. 4 was recorded after releasing the pressure from 7.8 GPa. Only below ≈ 2 GPa the NaCl phase was completely

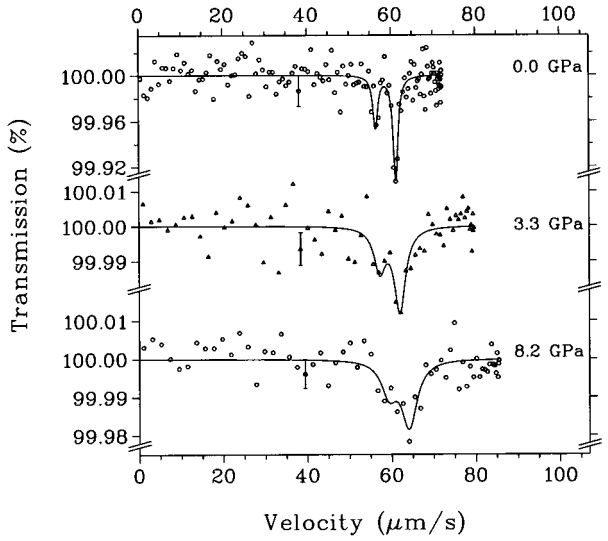

FIG. 3. Mössbauer absorption spectra of ^{67}ZnSe recorded at 4.2 K and three different pressures. Source: ^{67}GaZnO. Note the restricted range of Doppler velocities.

transformed back to the wurtzite structure.

The Lamb-Mössbauer factor f (LMF) can be derived from the total area under the absorption lines after correction for nonresonant background radiation if the effective absorber thickness is known. Our results on LMF in Table III also include an effective Debye temperature Θ_D derived from f assuming a Debye-type phonon frequency distribution. The LMF slightly increases with pressure. From Table III we get

$$f^{\text{wurtzite}}=[2.0+(0.046\pm 0.016)\cdot P]\%, \qquad (1)$$

where P is in GPa. The LMF is normalized to $f^{\text{wurtzite}}=2.0\%$ (Ref. 19) at ambient pressure. This value was obtained in more accurate experiments with the absorber outside of the high-pressure cell.

In the region of the phase transition, however, the situation becomes more complex: since both phases are present, their effective absorber thicknesses are unknown. We solved this problem by extrapolating Eq. (1) to pressures up to ≈ 8 GPa. The effective absorber thickness for that part of the sample which is still in the wurtzite phase can then be calculated from f^{wurtzite} and together with the total absorber thickness the effective thickness of the remaining part of the sample which already has been transformed to the NaCl structure can be derived. Using this procedure we obtain for the pressure dependence of the LMF of the NaCl phase

$$f^{\text{NaCl}}=[(2.38\pm 0.69)+(0.15\pm 0.12)\cdot P]\%. \qquad (2)$$

The spectrum obtained at 9.0 GPa (see Fig. 4, bottom) which we attribute to ZnO in the NaCl structure, was fitted by a superposition of a sharp and a broad Gaussian doublet. The linewidth of the broad doublet is rather large resulting in only a wide unresolved absorption dip. Both doublets exhibit the same center shift within experimental accuracy. For this reason both doublets belong to the NaCl phase of ZnO. The broad doublet originates from a distribution of hyperfine interactions which is present close to the phase transition.[30]

TABLE II. Results of the least-squares fits of the Mössbauer spectra of ^{67}ZnSe at various pressures P and corresponding volume compressions ($\Delta V/V_0=1-V/V_0$). Pos: position of the line with larger intensity; Γ: linewidth (FWHM); A: total absorption area beneath the Lorentzian doublet. The Lamb-Mössbauer factor (f) and the corresponding Debye temperature (Θ_D) are also given.

P (GPa)	0.0	3.3(1)	6.1(2)	8.2(3)
$\Delta V/V_0$ (%)	0.0	4.30(12)	7.30(19)	9.27(26)
Pos (μm/s)	61.14(8)	62.1(3)	62.7(8)	63.6(5)
Γ (μm/s)	1.4(2)	3.0(7)	9(2)	5(1)
A (%μm/s)	0.10(2)	0.18(3)	0.36(4)	0.18(3)
f (%)	0.50(6)	0.78(12)	1.19(20)	0.92(16)
Θ_D (K)	229(5)	250(8)	274(10)	259(9)

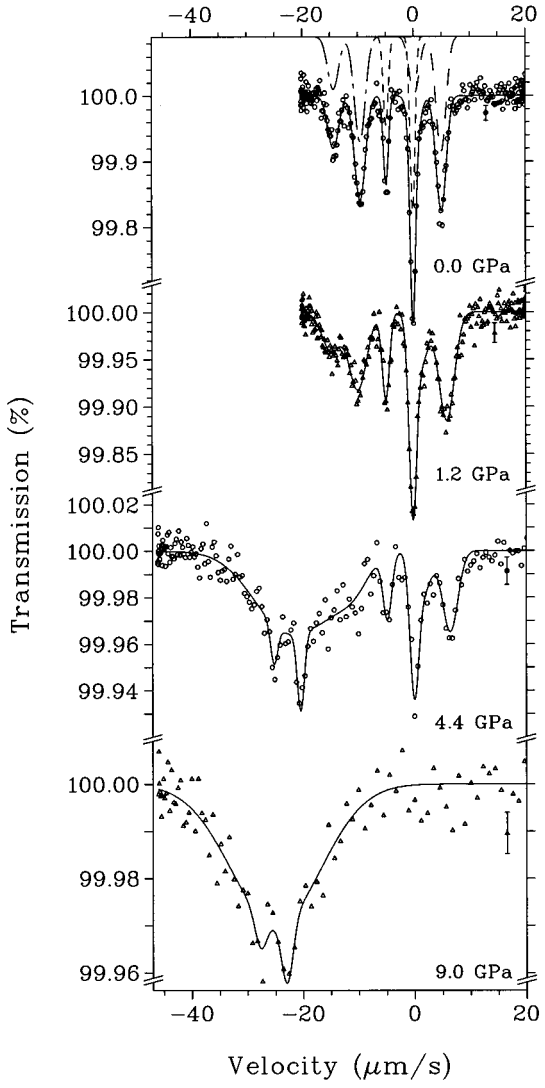

FIG. 4. Mössbauer absorption spectra of ^{67}ZnO recorded at 4.2 K and four different pressures. Source: ^{67}GaZnO. Note the restricted range of Doppler velocities.

TABLE III. Summary of measured Mössbauer parameters of ZnO (wurtzite) at different pressures P and corresponding volume compressions $\Delta V/V_0$. Pos_i: position of the line with larger intensity of doublet i ($i=1,2,3$); Γ_i: linewidth (FWHM) and A_i^{rel}: relative intensity of doublet i; S_C: center shift relative to ^{67}GaZnO source; f_Q: quadrupole frequency; η: asymmetry parameter; f: Lamb-Mössbauer factor; Θ_D: effective Debye temperature deduced from f.

P (GPa)	0	0.7(2)	1.2(2)	2.3(2)	3.5(3)	5.3(3)	6.4(3)	7.2(4)
$\Delta V/V_0$ (%)	0	0.38(10)	0.64(10)	1.22(10)	1.84(10)	2.70(10)	3.22(14)	3.58(19)
Pos_1 (μm/s)	−9.52(2)	−9.92(6)	−10.05(9)	−10.6(2)	−10.4(2)	−10.9(4)	−10.8(8)	−11.1(4)
Pos_2 (μm/s)	−0.126(9)	−0.22(2)	−0.22(2)	−0.25(4)	−0.18(3)	−0.09(4)	0.32(5)	0.31(5)
Pos_3 (μm/s)	5.03(2)	5.44(5)	5.86(6)	6.2(2)	7.1(1)	7.6(2)	7.7(3)	8.1(2)
Γ_1 (μm/s)	2.12(5)	3.2(1)	3.8(2)	5.0(6)	7.7(7)	10(1)	13(2)	8(1)
Γ_2 (μm/s)	1.05(2)	1.30(4)	1.50(5)	1.8(1)	2.09(7)	2.5(1)	1.8(1)	2.3(1)
Γ_3 (μm/s)	2.19(5)	2.88(9)	3.3(1)	4.4(3)	5.9(3)	6.3(4)	7.1(9)	5.1(4)
A_1^{rel}	0.327(5)	0.315(8)	0.321(9)	0.29(2)	0.27(1)	0.28(2)	0.28(3)	0.24(2)
A_2^{rel}	0.290(5)	0.295(8)	0.290(9)	0.33(2)	0.29(1)	0.30(2)	0.27(3)	0.34(2)
A_3^{rel}	0.381(6)	0.390(9)	0.39(1)	0.38(2)	0.43(1)	0.42(1)	0.45(3)	0.43(2)
S_C (μm/s)	0.05(1)	0.03(2)	0.12(4)	0.1(1)	0.36(9)	0.4(1)	0.7(3)	0.6(1)
f_Q (MHz)	2.393(5)	2.49(1)	2.55(2)	2.70(5)	2.71(5)	2.86(8)	2.93(18)	3.00(8)
η	0.284(9)	0.37(1)	0.45(2)	0.46(4)	0.58(3)	0.59(5)	0.53(10)	0.54(5)
f (%)	2.00	2.07(12)	2.21(12)	2.07(14)	2.16(10)	2.22(11)		
Θ_D (K)	310	313(5)	319(5)	313(5)	316(4)	319(4)		

Table IV summarizes the Mössbauer parameters for ZnO (NaCl structures) at various pressures.

Similar to the ZnSe system, the center shifts S_C of both phases of ZnO change only slightly with pressure (see Tables III and IV). All changes of EFG, S_C, and LMF are reversible, i.e., these parameters resume their original values after decompression to ambient pressure.

C. Lattice-dynamic calculations

In a recent publication[38] we have applied various lattice-dynamic models to calculate the Lamb-Mössbauer factors (LMF) and second-order Doppler shifts (SOD) for metallic as well as ionic zinc systems. Only few models have been published so far which describe pressure-dependent lattice-dynamic effects. For zinc chalcogenides the model of Talwar *et al.*[39] is available which provides the pressure dependence of force constants for ZnS, ZnSe, and ZnTe. It is a *rigid-ion model* with 11 independent parameters (RIM11).

Rigid-ion models describe the interaction between two ions in the crystal by two contributions: a short-range interaction between nearest neighbors (NN) and next-nearest neighbors (NNN) due to the covalent bonding and repulsive overlap forces and a long-range interaction due to the Coulomb forces between the ions. For the Coulomb interaction the ions are assumed to be point charges with no internal structure, i.e., rigid ions.

TABLE IV. Summary of Mössbauer parameters of ZnO (NaCl) at different pressures P and corresponding volume reductions $\Delta V/V_0$. The spectra at 8.9 and 9.7 GPa were measured when increasing pressure, before reaching the complete transformation of the sample to the NaCl structure. The pressure points at 7.8, 5.4, and 4.4 GPa were taken using a cell with sandwich gasket type I (see Sec. II) after decreasing the pressure from 7.8 GPa. In this case, the sample is only partly transformed to the NaCl phase. The pure NaCl phase was observed at pressures of 9.0 and 5.5 GPa after releasing the pressure from its maximum value of $\approx$10 GPa. The spectra consist of a superposition of a sharp and a broad doublet labeled $H1$ and $H2$, respectively. $A_{\mathrm{rel}}^{H_1}$ gives the area of the sharp doublet relative to the total ''cubic'' subspectrum. The center shifts $S_C^{H_1}$ and $S_C^{H_2}$ are relative to ^{67}ZnO (wurtzite) at ambient pressure. All other abbreviations as in Table III.

P (GPa)	4.4(3)	5.4(3)	5.5(1.0)	7.8(8)	8.9(1.4)	9.0(2.0)	9.7(1.7)
$\Delta V/V_0$ (%)	1.84(12)	2.24(12)	2.28(15)	3.16(15)	3.57(14)	3.60(18)	3.86(18)
Γ^{H_1} (μm/s)	1.5(3)	1.3(2)	2.0(4)	1.2(2)	1.6(8)	2.1(9)	2.0(5)
Γ^{H_2} (μm/s)	12.9(9)	11.4(6)	26(2)	13.9(7)	15(3)	18(1)	16(2)
Pos^{H_1} (μm/s)	−20.42(9)	−21.18(9)	−21.2(1)	−22.30(7)	−22.7(3)	−22.9(3)	−22.9(2)
Pos^{H_2} (μm/s)	−21.0(3)	−21.8(2)	−20.8(8)	−23.4(3)	−24(1)	−23.5(4)	−23.3(6)
$A_{\mathrm{rel}}^{H_1}$	0.13(3)	0.09(2)	0.14(3)	0.09(2)	0.14(8)	0.07(4)	0.17(5)
$S_C^{H_1}$ (μm/s)	−18.83(9)	−19.59(9)	−19.61(14)	−20.71(7)	−21.15(29)	−21.28(30)	−21.36(15)
$S_C^{H_2}$ (μm/s)	−19.4(3)	−20.2(2)	−19.2(8)	−21.8(3)	−22(1)	−21.9(4)	−21.7(6)
f (%)	3.05(25)	3.19(22)		3.56(31)			
Θ_D (K)	348(8)	362(7)		364(9)			

TABLE V. Pressure (volume) dependence of center shift S_C, second-order Doppler shift S_{SOD} and isomer shift S in ^{67}ZnSe. All values are given relative to ^{67}ZnSe at ambient pressure.

P (GPa)	3.3(1)	6.1(2)	8.2(3)
$1-V/V_0=\Delta V/V_0$(%)	4.30(12)	7.30(19)	9.27(26)
ΔS_C (μm/s)	0.9(3)	1.6(8)	2.4(5)
ΔS_{SOD}(RIM11) (μm/s)	−2.56	−4.54	−5.92
ΔS_{SOD}(Debye) (μm/s)	−4.9(21)	−10.5(26)	−7.0(21)
ΔS(RIM11)$=\Delta S_C-\Delta S_{SOD}$(RIM11) ($\mu$m/s)	3.5(3)	6.1(8)	8.3(5)
ΔS(Debye)$=\Delta S_C-\Delta S_{SOD}$(Debye) ($\mu$m/s)	5.8(21)	12.0(26)	10.7(21)

The parameters of RIM11 were adjusted to fit the Raman data for ZnSe at ambient pressure and at 13.7 GPa. A linear dependence of the model parameters was assumed for the pressure range in between.[40]

Unfortunately, there is no model available which describes the pressure dependence of force constants for ZnO. To calculate the SOD of ZnO at ambient pressure we have used the model of Ref. 41, which is tailored to the hexagonal (wurtzite) structure and allows us to take anisotropic effects into account.[38]

Concerning the numerical procedure, in a first step, the force constants are calculated from the model parameters. Then the dynamical matrix is calculated and the resulting eigenvalue problem solved at each point of a dense **q** mesh in the irreducible Brillouin zone.[42] For both zinc chalcogenides we chose a **q** mesh with 3680 points which we found to be sufficient to obtain good numerical accuracy and convergence. Further details are described in Ref. 38.

For the LMF of ZnSe at ambient pressure the RIM11 gives $f=0.420\%$ which is in good agreement with the experimental value of $f=(0.50\pm0.06)\%$ (see Table II). When pressure is increased the RIM11 predicts a continuous decrease of the LMF, in disagreement with experiment. This discrepancy will be discussed in Sec. IV B.

The pressure (volume) dependences of the experimentally observed center shift S_C, the calculated second-order Doppler shift S_{SOD}, and of the isomer shift $S=S_C-S_{SOD}$ in ^{67}ZnSe are summarized in Table V. It also includes the changes of the shifts which were obtained when the Debye model was used to calculate S_{SOD}.

D. Hartree-Fock cluster calculations

The all-electron Hartree-Fock (HF) cluster procedure has been applied to the study of ^{67}Zn isomer shifts at ambient pressure in a wide range of ionic compounds including ZnF_2 and all zinc chalcogenides.[16,43] In this method, the solid-state system is simulated by a finite number of ions (cluster), with the ion whose properties are being studied, in this case the zinc ion, at the center. The influence of the rest of the lattice is incorporated by including in the HF potential for the electrons in the cluster, the potential due to the ions outside the cluster, considering their influence to be described as that due to point charges. Thus the Madelung potential of the infinite solid has been included by embedding the cluster in an array of point charges with the same symmetry as the crystal. The HF cluster procedure includes covalency effects in a first-principles manner.[16] The core was not frozen, i.e., all electrons inside the cluster have been taken into account. A major drawback, however, is that the cluster which can be handled in this way, in rather small, although the rapid advance of computer technology will remedy this problem.

We have extended the *ab initio* HF calculations described in Ref. 16 to ZnSe (sphalerite structure) and ZnO (rocksalt structure) under external pressure. The clusters $(ZnSe_4)^{6-}$ and $(ZnO_6)^{10-}$ were used. The HF calculations were carried out employing contracted Gaussian-type functions. The basis sets used for zinc and the ligands were optimized for the neutral atoms as described in detail in Ref. 16. Table VI summarizes our results for ZnSe with reduced volume of the unit cell. We applied a scaling factor $S'(Z)=1.40$ to take relativistic effects into account.[16] The total s electron density $\rho(0)$ at the ^{67}Zn nucleus increases when the unit-cell volume of ZnSe is reduced. This increase is mainly due to the Zn($4s$) electron contribution and reflects the increase of covalency with pressure. The contributions of the $1s$, $2s$, and $3s$ shell nearly compensate each other (see Sec. IV B 2).

Table VII gives the results of the HF calculations for $\rho(0)$ in ZnO (NaCl structure). Contrary to the case of ZnSe, the inner core gives a sizable negative contribution which counteracts the positive contribution of the $4s$ electrons. This different behavior of ZnO (rocksalt structure) under pressure can also be noticed from Table VIII which compares the changes of the $4s$ electron density with the total s electron density at the ^{67}Zn nucleus in the zinc chalcogenides (see Sec. IV B 2).

The electric-field-gradient (EFG) tensor at the ^{67}Zn nucleus in ZnO (wurtzite) at ambient pressure has been calculated earlier[15] by the HF technique. The EFG tensor depends very sensitively on the oxygen parameter u (see Sec. IV B 2). Unfortunately, the pressure dependence of u is not known. For this reason a calculation of the EFG tensor with reduced unit-cell volume was not performed.

TABLE VI. Results of our HF calculations: Contribution of the $1s$, $2s$, $3s$, and $4s$ orbitals to the total s electron density $\rho(0)$ at the ^{67}Zn nucleus in ^{67}ZnSe (sphalerite) when the unit-cell volume is reduced by 0, 3, and 10%. $\Delta\rho(0)$ is the change of total s electron density relative to $\rho(0)$ in ^{67}ZnSe at ambient pressure.

	^{67}ZnSe		
$1-V/V_0=\Delta V/V_0$ (%)	0	3	10
Zn($1s$): (e/a_0^3)	22 562.58	22 562.57	22 562.53
Zn($2s$): (e/a_0^3)	2 294.88	2 294.87	2 294.87
Zn($3s$): (e/a_0^3)	328.68	328.69	328.75
Zn($4s$): (e/a_0^3)	5.28	5.46	5.88
$\Delta\rho(0)$ (e/a_0^3)	0	0.17	0.61

TABLE VII. Results of our HF calculations: Contributions of the $1s$, $2s$, $3s$, and $4s$ orbitals to the total s electron density $\rho(0)$ at the ^{67}Zn nucleus in ^{67}ZnO (NaCl structure). Under compression of $\Delta V/V_0 = 4.8\%$ the s electron density increases by $\Delta\rho(0) = 0.10 e/a_0^3$.

$1 - V/V_0 = \Delta V/V_0$ (%)	0	4.8
Zn($1s$): (e/a_0^3)	22 562.71	22 562.69
Zn($2s$): (e/a_0^3)	2 294.78	2 294.78
Zn($3s$): (e/a_0^3)	328.08	328.05
Zn($4s$): (e/a_0^3)	3.15	3.30
$\Delta\rho(0)$ (e/a_0^3)	0	0.10

E. LAPW band-structure calculations

Our band-structure calculations employ the full-potential linearized-augmented plane-wave (LAPW) method based on density-functional theory.[44–46] The crystallographic structure is required as experimental input. A fully relativistic description for the core states, but a scalar-relativistic description, neglecting spin-orbit coupling, for the valence states is used. Exchange and correlation is taken into account within the local-density approximation, where the exchange potential is determined by the electron density in the crystal. This density is calculated self-consistently. The electric-field-gradient (EFG) tensor is derived directly from the charge density in an *ab initio* procedure.

We employ a well converged basis using $R_{mt}K_{\max} = 8.5$, where R_{mt} denotes the smallest atomic sphere radius and $K_{\max}$ gives the magnitude of the largest K vector in the plane-wave expansion. We treat the O $2s$, $2p$ and the Zn $3d$, $4s$, $4p$ orbitals as valence states and all lower-lying states as core. To improve upon the linearization local orbitals[47] for O $2s$ and Zn $3d$ states were added to the standard LAPW basis. In contrast to TiO_2, where the Ti $3p$ states were found to contribute significantly to the EFG,[47] the localized and deep-lying Zn $3p$ states have a negligible effect on the EFG. Self-consistency was reached using eight special k points.

We have used this method to calculate electron densities at the ^{67}Zn nucleus in ZnO (wurtzite and rocksalt structures) for several volumes. In the wurtzite structure for each volume the c/a ratio as well as the oxygen parameter u were optimized by minimization of the total energy.

Also our LAPW calculations show that the EFG tensor in ZnO (wurtzite) strongly depends on the oxygen parameter u. Details will be discussed in Sec. IV B 2. Since the pressure dependence of u is not known, a detailed calculation of the EFG in ZnO (wurtzite) cannot be carried out.

TABLE VIII. Results of our HF calculations: Volume dependence of the $4s$ electron density, $\Delta\rho^{4s}(0)/(\Delta V/V_0)$ and of the total s electron density at the ^{67}Zn nucleus in ZnO (NaCl structure) and ZnS, ZnSe, and ZnTe (all sphalerite structure). $\Delta\rho^{4s}(0)$ and $\Delta\rho(0)$ are given in units of e/a_0^3.

	ZnO	ZnS	ZnSe	ZnTe
Zn($4s$): $\Delta\rho^{4s}(0)/(\Delta V/V_0)$	−3.1	−5.6	−6.0	−5.7
Total: $\Delta\rho(0)/(\Delta V/V_0)$	−2.1	−5.6	−6.1	−6.2

IV. DISCUSSION

A. Crystallographic phase transitions in Zn chalcogenides

The volume change $1 - V_{0H}/V_0$ at the phase transition is found to be the same ($\approx 18.3\%$) for the three systems ZnO, ZnS, and ZnSe when extrapolating the parameters of the high-pressure phase to ambient pressure (see Table I and Sec. III). At this drastic volume collapse the nearest-neighbor (NN) distance increases by $\approx 8\%$, the next-nearest-neighbor (NNN) distance, however, decreases by $\approx 6.5\%$ and the coordination number is changed from four to six. The hysteresis of the phase transition is most strongly pronounced in ZnO. All changes are reversible when pressure is released completely. Since the pressure is applied at room temperature where the methanol-ethanol solution is in the liquid phase and pressure gradients are smaller than 10% even at cryogenic temperatures (see Sec. II), non-hydrostatic pressure conditions are responsible only to a minor extent for the large hysteresis observed. It appears that the large hysteresis is rather an intrinsic property of zinc chalcogenides.

To describe the phase transitions several semiempirical models have been used.[8–10,48,49] Such models emphasize the concepts of ionicity and bond length. Only recently has it been possible to perform *ab initio*-type calculations on ZnO (wurtzite structure).[13,14] We have carried out scalar-relativistic (spin-orbit coupling is neglected) linearized-augmented plane-wave (LAPW) calculations[44] for this compound. Table IX compares relevant experimental results with the present LAPW calculations and other theoretical models from literature. For ZnO almost quantitative agreement between experiment and theoretical LAPW calculations is achieved, but also the *ab initio* Hartree-Fock calculations[13,14] and semiempirical calculations[8,49] obtained very accurate results, although the transition pressure varies significantly between the theoretical models.

B. Mössbauer effect measurements

Due to the high sensitivity of the ^{67}Zn resonance even to small changes of hyperfine interactions[19] the linewidth in ^{67}Zn Mössbauer experiments is strongly affected by distributions of isomer shifts and/or electric-field gradients. Such distributions of hyperfine interactions may arise from pressure gradients across the sample. Although pressure gradients were found to be smaller than 10% in our experiments (see Sec. II) they are a major cause of the line broadening observed. In addition, close to the phase transitions the phases may be ill-defined crystallographically resulting again in distributions of hyperfine interactions. Such a situation exists, for example, in ZnO at 9.0 GPa (see Fig. 4 bottom, Sec. III B 2) where in addition to a sharp doublet a broad unresolved peak at the same center shift S_C is observed. However, since the energy resolution of the ^{67}Zn resonance is very high, line broadening usually is not a problem when determining hyperfine interactions. Also the LMF is hardly affected, because it depends on the total *area* beneath the absorption spectrum. For these reasons the pressure dependencies of linewidths will not be discussed further in this paper.

1. Lamb-Mössbauer factor

ZnSe. Tables II and V summarize our results for ZnSe. Figure 5 depicts the pressure (volume) dependence of the

TABLE IX. Experimental structural parameters compared to results of theoretical calculations for zinc chalcogenides. B_0, B_0': bulk modulus and its pressure dependence of the ambient-pressure phase; B_{0H}, B_{0H}' bulk modulus and its pressure dependence of the high-pressure phase; u: oxygen parameter; P_T: transition pressure; $\Delta V/V_0$: relative volume difference between the two phases extrapolated to ambient pressure; ΔE_0: difference in cohesion energy between the two phases.

		ZnO	ZnS	ZnSe
		Ambient-pressure phase:		
B_0 (GPa)	Expt.	183(7)	75.0(2.0) [a]	69.3(1.1)
	Theor.	173 [b], 154.4 [c], 160 [d]	69 [b], 75.9 [e]	53 [b]
B_0'	Expt.	4 (fix)	4 (fix)	4 (fix)
	Theor.	3.6 [c], 4.4 [d]	4.7 [e]	
c_0/a_0	Expt.	1.6018(7)		
	Theor.	1.593 [c], 1.604 [d]		
$d(c/a)/dp$ (GPa^{-1})	Expt.	$-0.0007(3)$		
	Theor.	-0.0005 [c]		
u	Expt.	0.3819(1) [f]		
	Theor.	0.3856 [c], 0.381 [d]		
		High-pressure phase:		
B_{0H} (GPa)	Expt.	228(7)	104(6) [a]	104(6)
	Theor.	204 [b], 203.3 [c], 205 [d]	80 [b], 83.1 [e]	62 [b]
B_{0H}'	Expt.	4 (fix)	4 (fix)	4 (fix)
	Theor.	3.6 [c], 4.88 [d]	10.0 [e]	
P_T (GPa)	Expt.	2.0–8.7	10.0–14.7 [a]	9.5–13.0
	Theor.	3.6 [b], 8.57 [c], 14.5 [d]	4.7 [b], 16.1 [e]	4.4 [b]
$\Delta V/V_0$ (%)	Expt.	18.13(10)	18.3(1.0) [a]	18.6(5)
	Theor.	19.42 [c], 17.9 [d]		
ΔE_0 (meV)	Expt.	53–225		390–490
	Theor.	242 [c], 160 [d]		

[a]Reference 5.
[b]Reference 8.
[c]Reference 14.
[d]LAPW calculation of this work.
[e]Reference 13.
[f]Reference 58.

LMF. When the unit-cell volume is reduced, the LMF first increases from $f=(0.50\pm0.06)\%$ at ambient pressure to $f=(1.19\pm0.20)\%$ at 6.1 GPa. Increasing the pressure further, a nearly linear increase of the LMF to $f\approx1.25\%$ at 8.2 GPa is to be expected. Such a linear dependence has been found, e.g., for brass alloys.[21] In ZnSe, however, the LMF drops again to $f=(0.92\pm0.16)\%$ at 8.2 GPa, although the crystallographic phase transition (≈13 GPa) has not yet been reached. This behavior can be compared to the predictions of an 11-parameter lattice-dynamic model (RIM11).[39]

According to RIM11, in general the frequencies of most phonon modes *increase* when the unit cell is compressed. This is mainly due to the strong increase of the repulsive component of the ion-ion interaction when the ion separation is diminished. In some compounds, e.g., in zinc chalcogenides, however, certain frequencies are *reduced*. In II-VI systems with zinc-blende structure this is the case for the transverse acoustic (TA) modes. This mode softening is not caused by the NN interaction but is due to the decrease of NNN interaction with reduced volume.[42] In fact, the contribution of the NN interaction to the LA and optical modes strongly increases with reduced volume. The contribution of the NN interaction to the frequency of the TA modes remains virtually unaffected, since in these modes less stretching of the NN bonds occurs. The contribution of the NNN interaction, however, *decreases* for all modes due to increased screening of the Coulomb force between the zinc ions by the bonding electrons when the volume is diminished. Thus, the total effect is a reduction of the frequencies of the TA modes.

The crystallographic phase transition occurs when bonding electrons have screened the repulsive NNN interaction to such an extent that the attractive NN interaction cannot be compensated anymore. A similar situation has been found for GaAs,[50] where the softening of the TA mode is followed by a phase transition into an orthorhombic structure. As seen in Fig. 5, the LMF at ambient pressure is well reproduced by RIM11. This is not true for higher pressures. The model predicts a continuous decrease. A linear pressure dependence of the model parameters between ambient pressure at 13.7 GPa might be too crude an approximation. Still, RIM11 gives a hint in which way the crystallographic phase transi-

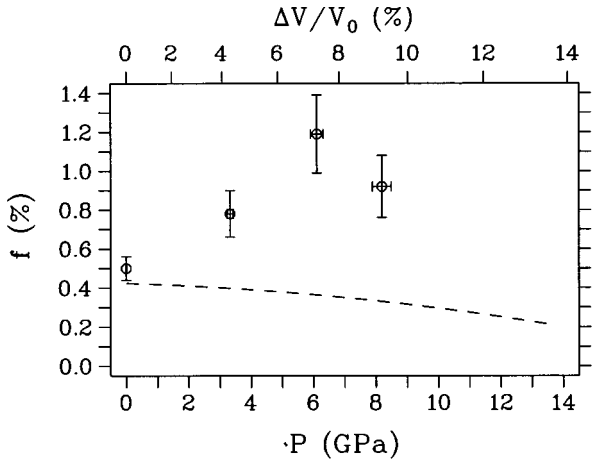

FIG. 5. Pressure dependence of the LMF for ^{67}ZnSe; ○: experimental values; – – – prediction of a lattice-dynamic model (RIM11).

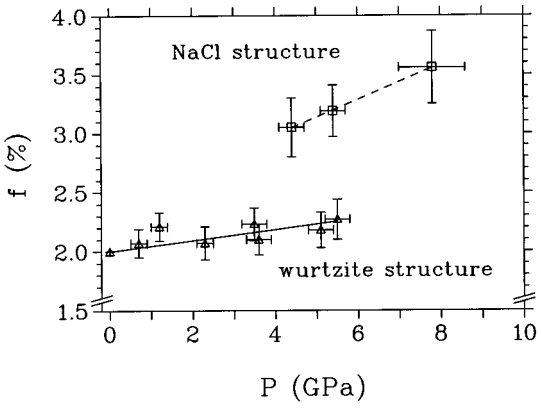

FIG. 6. Pressure dependence of the LMF's for both phases of ^{67}ZnO. The straight-line fits give: $f^{\text{wurtzite}}=[2.0+(0.046\pm0.016)\cdot P]\%$ and $f^{\text{NaCl}}=[(2.38\pm0.69)+(0.15\pm0.12)\cdot P]\%$, with P in GPa.

tion is reflected in the phonon modes much below the transition. For the description of the experimental LMF data, however, more detailed information on the pressure dependence of the model parameters is required. Experimentally the pressure range in Mössbauer measurements has to be increased to cover the regime of the phase transition.

ZnO. For this compound we were able to cover the pressure range of the crystallographic transition (see Tables III and IV, Sec. III). Figure 6 summarizes the pressure dependence of the LMF in both phases.

The NaCl phase of ZnO exhibits a considerably larger LMF than the wurtzite structure and also the pressure dependence appears to be increased. This is consistent with the larger B_0 value. Since the NN distance is larger in the NaCl than in the wurtzite structure this increase of LMF and B_0 reflects the higher coordination number of zinc in the NaCl structure. Within both phases the LMF rises with pressure due to the increase of covalency of the chemical bond when the NN distance is reduced. Contrary to ZnSe, in ZnO we observe no decrease in f or changes in SOD which could be attributed to mode softening in the neighborhood of the phase transition.

2. Hyperfine interactions

Isomer shift in ZnSe. The isomer shift S is proportional to the electron density $\rho(0)$ at the ^{67}Zn nucleus (mainly s electrons). The second-order Doppler shift S_{SOD} which is proportional to $\langle v^2\rangle$, the mean-square velocity of the ^{67}Zn nucleus at its equilibrium position, is a lattice-dynamic property. With ^{67}Zn-Mössbauer spectroscopy, S and S_{SOD} can be of the same magnitude and it can be difficult to separate the two contributions.[19,51] We have tried two methods: (a) assuming that the Debye approximation holds we calculated an effective Debye temperature Θ_D from our result for the LMF and using the same Θ_D we derived S_{SOD}; (b) we employed the more realistic lattice-dynamic models for ZnO (Ref. 41) and ZnSe,[39] which gave reasonable results for the LMF (see Sec. IV B 1) to calculate SOD for ZnO at ambient pressure and for ZnSe over the whole pressure range investigated. At ambient pressure, the Debye model gives $S_{\text{SOD}}(\text{Debye})=19$ μm/s, from the more advanced models we obtain $S_{\text{SOD}}(\text{RIM11})=(25\pm8)$ μm/s between ZnO (wurtzite) and ZnSe. The rather large uncertainty ±8 μm/s which covers also the result of the Debye model is an estimate of possible systematic errors originating from insufficiencies within the force-constant models.[38,42]

For the isomer shift at ambient pressure we obtain $S=S_C-S_{\text{SOD}}=(62.7-25)$ μm/s$\approx(38\pm8)$ μm/s. Using $\Delta\langle r^2\rangle=+(13.9\pm1.4)\times10^{-3}$ fm^2,[16] this corresponds to an increase $\Delta\rho(0)=(1.38\pm0.32)e/a_0^3$ in ^{67}ZnSe as compared to ^{67}ZnO (wurtzite). This is in good agreement with results from previous *ab initio* Hartree-Fock (HF) cluster calculations,[16] where $\Delta\rho(0)=(1.53\pm0.15)e/a_0^3$ for the change of $\rho(0)$ between ^{67}ZnO and ^{67}ZnSe was obtained. The HF calculations show that the increase of $\rho(0)$ between ZnO and ZnSe is due to the higher covalency of the chemical bond in ZnSe as compared to ZnO. With respect to the purely ionic state (Zn^{2+}) covalency increases population of zinc $4s$ and $4p$ electronic states. It also affects the $3s$ core, but in a more subtle way.[16] It turns out that Zn($4s$) valence orbitals contribute $\approx70\%$ to $\Delta\rho(0)$, Zn($3s$) orbitals $\approx30\%$, whereas the Zn($1s$) and Zn($2s$) core electrons remain virtually unaffected.

When pressure on ^{67}ZnSe is increased the change of S_C is rather small (see Tables II and V in Sec. III). Using again the RIM11,[39] as well as the Debye approximation, we have calculated the pressure (volume) dependence of S_{SOD}. In both models the increase of S with pressure $[\Delta S(\text{RIM11}),\Delta S(\text{Debye})]$ is partially compensated by the decrease of S_{SOD}. This compensation is the reason for the small variation of S_C.

We have extended our *ab initio* HF calculations to ZnSe with reduced volume of the unit cell (see Sec. III D, Table VI). As expected, when the unit-cell volume of ZnSe is reduced, covalency strongly increases. This is directly reflected in the sharp increase of the Zn($4s$) contribution which linearly scales with $1/(V/V_0)$ up to volume changes of $V/V_0=0.9$. Figure 7 summarizes our experimental and theoretical results for the changes of S_C, S_{SOD}, and S with reduced volume. It appears that the theoretical change of iso-

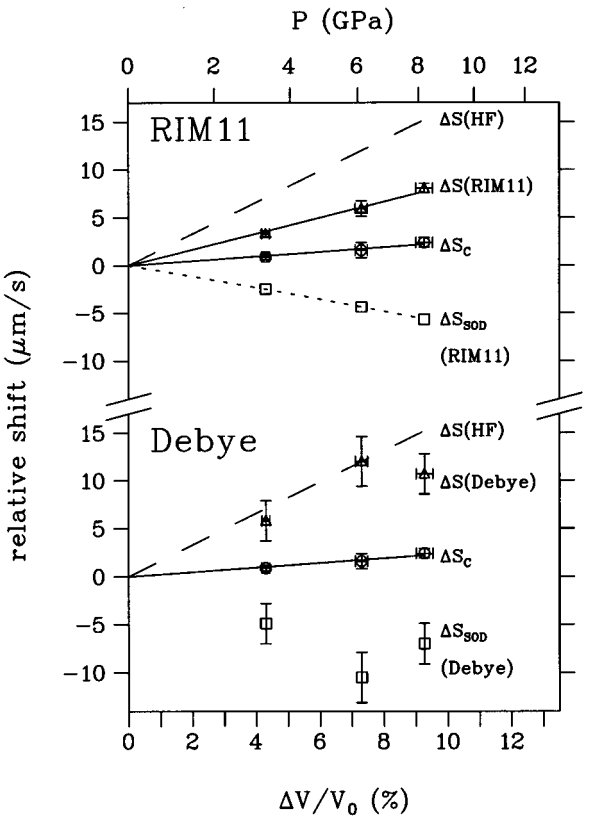

FIG. 7. Volume dependence of center shift S_C (circles), second-order Doppler shift S_{SOD} (squares) and isomer shift S (triangles) in ^{67}ZnSe; $\Delta S = \Delta S_C - \Delta S_{\mathrm{SOD}}$. All values are relative to ^{67}ZnSe at ambient pressure. ΔS(HF) indicated by the dashed line is the theoretical change of isomer shift derived from Hartree-Fock cluster calculations. ΔS(RIM11) and ΔS(Debye) are the changes of isomer shift when ΔS_{SOD} has been determined from RIM11 and the Debye model, respectively. Effective Debye temperatures were taken from Table II.

mer shift ΔS(HF) is far outside of ΔS(RIM11), where ΔS_{SOD}(RIM11) has been determined from RIM11, but is in fair agreement with ΔS(Debye), where the Debye approximation has been used. As already mentioned above, RIM11 is probably not sufficient to describe the volume dependences of LMF and SOD because the model parameters have been assumed to be linearly dependent on pressure. Our results suggest that RIM11 underestimates the increase of most phonon frequencies and thus gives too small a rise and drop for the LMF and SOD, respectively. The better agreement of experiment with theory when the Debye model is applied, is most probably fortuitous. The decrease of the LMF is caused by softening of low-frequency modes, whereas other phonon frequencies increase with reduced volume. Since the low-temperature limit the weighting factors of the phonon frequency distribution are ω^{-1} and ω^{+1} for LMF and SOD, respectively, the influence of low-frequency phonons on the SOD is expected to be less pronounced. It is overcompensated by the hardening of high-frequency phonons which causes ΔS_{SOD} to become more negative. For a reliable calculation of ΔS_{SOD} a more profound lattice-dynamic model is necessary. This in turn would make it possible to check our

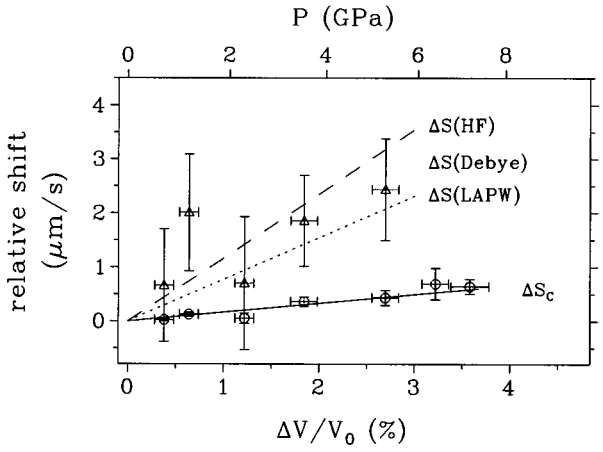

FIG. 8. Experimental change of center shift ΔS_C (circles) and calculated changes of isomer shift in ^{67}ZnO (wurtzite). All values are relative to ^{67}ZnO at ambient pressure. ΔS(HF) indicated by the dashed line and ΔS(LAPW) indicated by the dotted line are derived from Hartree-Fock and linearized augmented plane-wave calculations, respectively. ΔS(Debye) indicated by triangles represents the change in isomer shift when the second-order Doppler shift ΔS_{SOD} has been determined from the Debye model. Effective Debye temperatures were taken from Table III.

Hartree-Fock cluster calculations.

Isomer shift in ZnO. Again the problem of determining S_{SOD} arises. Since there is no advanced model available to describe the lattice dynamics of ZnO under pressure we used the Debye approximation with effective Debye temperatures listed in Tables III and IV. As demonstrated in Fig. 8 for ZnO (wurtzite), the center shift S_C changes only little with pressure. This is due to a close compensation of ΔS by ΔS_{SOD}, similar to the case of ZnSe. Since the variation of the oxygen parameter u with pressure is not known we performed LAPW calculations assuming u and the c/a ratio to be independent of pressure (see Secs. III A and III E). The dotted line ΔS(LAPW) in Fig. 8 indicates the calculated increase of S when the unit-cell volume is reduced. The dashed line ΔS(HF) is an estimate where the $4s$ electron density obtained from a HF calculation[16] is linearly scaled by (V_0/V). This estimate is based on the assumption that the $4s$ density provides the largest contribution to $\Delta\rho(0)$ because of covalency of the chemical bond (see Sec. III D, Table VIII). ΔS(Debye) lies between ΔS(HF) and ΔS(LAPW) indicating that the Debye approximation might be good enough for evaluating ΔS_{SOD} in ZnO (wurtzite) under pressure.

Figure 9 summarizes our result for ZnO in the NaCl phase. All shifts are given relative to ZnO (wurtzite) at ambient pressure. The center shift S_C is further reduced when pressure is increased. When the SOD is calculated within the Debye model S_{SOD} overcompensates S(Debye) which increases only slightly. Also the results of theoretical calculations, S(LAPW) and S(HF), confirm that the increase of S with pressure is considerably smaller as compared to the situations in ZnO (wurtzite) and ZnSe. There are mainly two reasons for this difference in behavior. Covalency and Zn $(4s)$ contribution to $\rho(0)$ are reduced due to the larger Zn-O

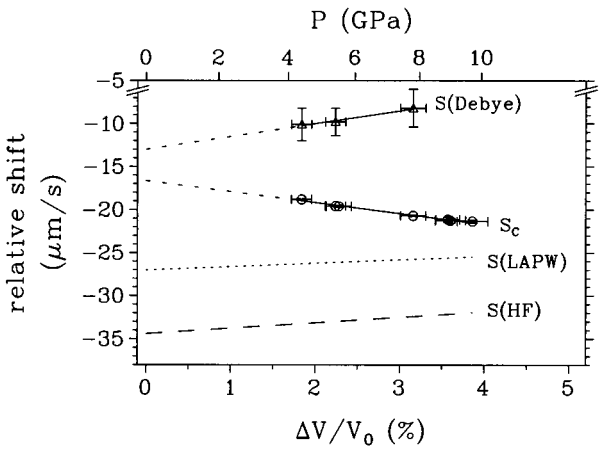

FIG. 9. Experimental center shift S_C (circles) and isomer shift S of ^{67}ZnO (NaCl structure). S(Debye) indicated by triangles is obtained when the second-order Doppler shift is estimated in the Debye approximation using the Debye temperatures of Table IV. S(HF) and S(LAPW) originate from theoretical calculations (see text). All shifts are given relative to ZnO (wurtzite) at ambient pressure.

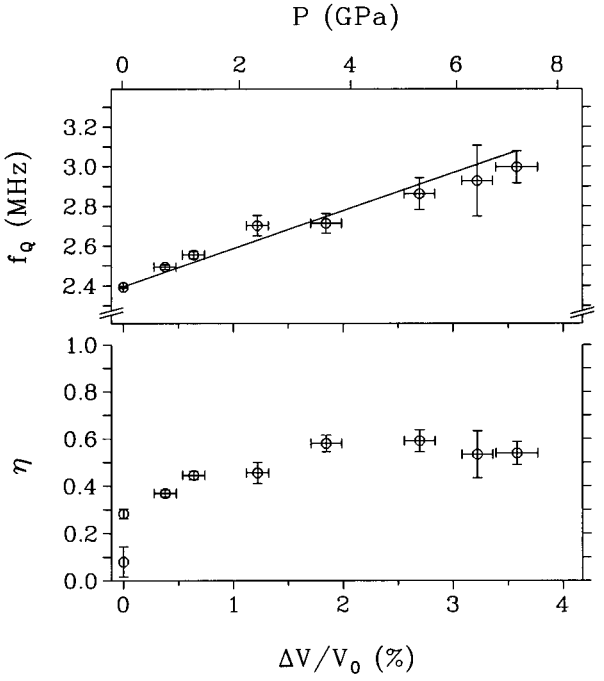

FIG. 10. Experimental values for quadrupole frequency f_Q and asymmetry parameter η of ^{67}ZnO (wurtzite) at 4.2 K under external pressure. The solid line is a straight-line fit to the f_Q data.

separation in ZnO (NaCl) as compared to ZnO (wurtzite). This is expected to lead to a smaller increase of $\rho(0)$ with pressure for ZnO (NaCl). In addition, our HF cluster calculations (see Sec. III D, Tables VI and VIII show that ZnS, ZnSe, and ZnTe (all sphalerite structure) behave very similarly with pressure: the negative contributions of the 1*s* and 2*s* electron shells are nearly compensated by the positive contribution of the 3*s* shell. Thus the total pressure dependence in these systems is almost completely determined by the 4*s* electrons. The situation appears to be quite different, however, for ZnO in the NaCl structure. Here the 1*s*, 2*s*, *and* 3*s* shells exhibit negative contributions which amount to $\approx 1/3$ of the positive contribution of the 4*s* electrons[52] (see Sec. III D, Table VII). As a consequence, the method of ''freezing'' inner core electrons can give wrong answers when changes of $\rho(0)$ are calculated and should be abandoned.

Figure 9 shows that the absolute values of S(LAPW) and S(HF) between ZnO (wurtzite) and ZnO (NaCl) are in agreement within $\approx 25\%$, whereas the results for S(Debye) are much more positive. We attribute this discrepancy mainly to the Debye approximation when determining S_{SOD}. In particular, the Debye model may be insufficient, when S_{SOD} is estimated between samples of different lattice structures. In order for S to agree with the theoretical calculations, the second-order Doppler shift (SOD) has to be more positive in ZnO (NaCl) than in ZnO (wurtzite). For the LMF, however, we find from experiment that $f^{\mathrm{NaCl}} > f^{\mathrm{wurtzite}}$. Taking the different frequency weighting factors for LMF and SOD into account, we are forced to the conclusion that on the one side low-frequency acoustic-phonon modes become harder and on the other side high-frequency optic modes become softer in ZnO (NaCl).

Indeed, mode softening of transverse-optical (TO) phonons has been predicted[8,49] for various systems at the phase transition from sphalerite to NaCl structures. For ZnO with hypothetical sphalerite structure a drastic drop in frequency of the TO mode at the Γ point from 18.8 THz (sphalerite) to 1.8 THz (NaCl) is calculated.[8,49] Since sphalerite and wurtzite structures exhibit similar bonding characteristics such a mode softening may also occur for ZnO (wurtzite) at the transition to the NaCl phase. For a more quantitative analysis, however, more advanced lattice-dynamic models are required.

Electric-field gradient in ZnO. The Zn site in ZnO (wurtzite) is expected to exhibit axial symmetry with respect to the *c* axis. As a consequence, the asymmetry parameter η of the electric-field-gradient (EFG) tensor should be $\eta = 0$. Experimentally, $\eta = 0$ is observed only with ZnO single crystals. Surprisingly, in ZnO powder $\eta \approx 0.1$, even at ambient pressure.[53] The pressure dependence of the EFG tensor is shown in Fig. 10. The quadrupole coupling frequency $f_Q = eQV_{zz}/h$ increases only slightly when the volume is reduced: $f_Q = [(2.396(12) + 19(2)\cdot(1 - V/V_0)]$ MHz. Using $Q = 0.150(15)b$ for the nuclear quadrupole moment of the spin-5/2 ground state of ^{67}Zn, we obtain for the main component V_{zz} of the EFG tensor: $V_{zz} = [0.66(7) + 5.2(8)\cdot(1 - V/V_0)] \times 10^{17}$ V/cm^2. Most striking, however, is the sharp rise of η to $\eta \approx 0.3$ already at very modest pressures (< 0.1 GPa). At higher pressures the asymmetry parameter saturates at $\eta \approx 0.6$. Our measurements clearly point out that the wurtzite structure is highly unstable against nonaxial lattice distortions. These distortions are so small that we failed to detect them via x rays.

For ZnO (wurtzite) results of HF cluster calculations[15,43] have been available. In addition, we performed LAPW calculations (see Sec. III E). The results for V_{zz} at ambient pressure are $+0.69 \times 10^{17}$ V/cm^2 (HF) and $+0.85 \times 10^{17}$

V/cm^2 (LAPW), both in good agreement with experiment $[+0.66(7)\times10^{17}\ V/cm^2]$. The dominant contribution to V_{zz} originates from the unbalanced occupation of the Zn $(4p)$ orbitals in the valence states, whereas the Zn$(3p)$ and the Zn$(3d/4d)$ orbitals give only a small (negative) contribution. The Zn$(2p)$ contribution can be neglected altogether. These results clearly emphasize the importance of covalency effects in the Zn-O bond. Also the decrease in the Zn charge from formally $+2.0$ to a Mulliken charge of $+1.62$ is almost entirely due to an increase in the Zn$(4p)$ electron population.

V_{zz} turns out to react very sensitively to details of the crystallographic structure, in particular to variation in the oxygen parameter u. We obtain from our Hartree-Fock and LAPW calculations $\Delta V_{zz}/\Delta u = 263\times10^{17}\ V/cm^2$ and $231\times10^{17}\ V/cm^2$, respectively. Our LAPW calculations show that the experimentally observed increase in V_{zz} with pressure (see Fig. 10) can only be accommodated if in addition to changes of the unit-cell volume and of the c/a ratio an increase of u is allowed for. For example, a volume change of $\Delta V/V_0 \approx 3.4\%$ (corresponding to $P \approx 6.8$ GPa) *alone* increases V_{zz} by $\approx 1.2\%$ only. If solely the c/a ratio is decreased by $\approx 5\times10^{-3}$ [again corresponding to $P \approx 6.8$ GPa (see Table IX)] V_{zz} *decreases* by $\approx 16\%$. Thus an increase of u appears to be essential. Still, the main problem is that $\eta \neq 0$, which means that the Zn atom moves off the symmetry axis. Unfortunately, up to now the distortions of the lattice which lead to $\eta \neq 0$ have not been determined experimentally. This has prevented a detailed calculation of the EFG tensor.

C. Electrical conductivity

At ambient pressure zinc chalcogenides represent semiconductors with rather large direct band gaps E_g, which increase with pressure.[54,55] In ZnSe for example, E_g increases monotonically from $E_g = 2.7$ eV at ambient pressure to 3.4 eV at 12 GPa.[5] The zinc chalcogenides with sphalerite structure, ZnS, ZnSe, and ZnTe, however, show a drastic increase of electrical conductivity by 6–8 orders of magnitude at the transition to the NaCl phase.[2,7,36] The nature of this drastic change has been discussed controversially. Optical measurements on ZnS (Refs. 5 and 6) have been interpreted in terms of an indirect semiconductor in accordance with recent theoretical results.[13] The increased conductivity has been attributed to a high defect concentration.

A theoretical study[56] on ZnSe implied that, also in this compound, a transition into an indirect semiconductor occurs. Optical measurements,[55,57] however, and in particular most recent high-pressure conductivity experiments[7] strongly favor the occurrence of a metallic state in the high-pressure NaCl phase of ZnSe. Such a metallic state is expected to clearly show up in Mössbauer effect measurements by a considerably *increased* s electron density $\rho(0)$ at the ^{67}Zn nucleus. Zn metal and brass alloys, for example, exhibit isomer shifts which are—relative to ZnSe—about 50 μm/s more positive. Unfortunately, we have not been able to reach the phase transition in Mössbauer experiments.

Our experimental and theoretical results on ZnO, however, prove this compound to behave quite differently from ZnSe: in the NaCl phase $\rho(0)$ is drastically *reduced*. Although conductivity measurements on ZnO are still missing, the low value for $\rho(0)$ suggests that ZnO remains nonmetallic. This is in accordance with a band gap of 1.36 eV obtained by a HF calculation.[18] Our theoretical LAPW calculations give an indirect gap of only 0.9 eV. However, it is well known that gaps in the local-density approximation are underestimated by about 50%. Therefore, also the LAPW calculations favor a nonmetallic state for ZnO in the NaCl phase.

V. CONCLUSIONS

^{67}Zn-Mössbauer spectroscopy at high external pressures is a powerful tool to study lattice-dynamic effects as well as hyperfine interactions. In ZnSe the LMF is strongly influenced by soft modes which appear already much below the crystallographic transition to the high-pressure NaCl structure. Also in ZnO soft modes play an important role. Here, however, they affect much more the second-order Doppler shift than the LMF. Our theoretical HF-cluster and LAPW calculations prove that in ZnSe and ZnO covalent contributions to the chemical bond are essential. They determine the EFG tensor in ZnO (wurtzite) as well as the s electron density $\rho(0)$ at the ^{67}Zn nucleus in the different crystallographic phases and the increase of $\rho(0)$ when the unit-cell volume is reduced. ZnO (wurtzite) is highly unstable even against small nonaxial lattice distortions. Such distortions which might be too tiny to be detected by x-ray analysis or neutron diffraction can clearly be discerned via the asymmetry parameter of the EFG tensor.

ACKNOWLEDGMENTS

We would like to thank the Forschungszentrum Karlsruhe, especially Dr. H. Schweickert, K. Assmus, and W. Maier for numerous and careful source irradiations at the cyclotron. This work has been funded by the German Federal Minister for Research and Technology [Bundesminister für Forschung und Technologie (BMFT)] under Contract No. 03-KA3TUM-4 and by the Forschungszentrum Karlsruhe.

*Present address: Pacific Northwest Laboratory, Dept. of Chemical Sciences, Richland, WA 99352.

[1] G. F. Neumark, R. M. Park, and J. M. DePuydt, Phys. Today **47**(6), 26 (1994), and references therein.
[2] G. A. Samara and H. G. Drickamer, J. Phys. Chem. Solids **23**, 457 (1962).
[3] C. H. Bates, W. B. White, and R. Roy, Science **137**, 993 (1962).
[4] P. L. Smith and J. E. Martin, Phys. Lett. **19**, 541 (1965).
[5] S. Ves, U. Schwarz, N. E. Christensen, K. Syassen, and M. Cardona, Phys. Rev. B **42**, 9113 (1990).
[6] Y. Zhou, A. J. Campbell, and D. L. Heinz, J. Phys. Chem. Solids **52**, 821 (1991).
[7] G. Itkin, G. R. Hearne, E. Sterer, M. P. Pasternak, and W. Potzel, Phys. Rev. B **51**, 3195 (1995).
[8] J. A. Majewski and P. Vogl, Phys. Rev. B **35**, 9666 (1987).
[9] J. R. Chelikowsky, Phys. Rev. B **35**, 1174 (1987).

[10] N. E. Christensen, Phys. Scr. T **19**, 298 (1987).
[11] M. Causa, R. Dovesi, C. Pisani, and C. Roetti, Phys. Rev. B **33**, 1308 (1986).
[12] P. Schröer, P. Krüger, and J. Pollmann, Phys. Rev. B **47**, 6971 (1993).
[13] J. E. Jaffe, R. Pandey, and M. J. Seel, Phys. Rev. B **47**, 6299 (1993).
[14] J. E. Jaffe and A. C. Hess, Phys. Rev. B **48**, 7903 (1993).
[15] D. W. Mitchell, S. B. Sulaiman, N. Sahoo, T. P. Das, W. Potzel, and G. M. Kalvius, Phys. Rev. B **44**, 6728 (1991).
[16] D. W. Mitchell, T. P. Das, W. Potzel, G. M. Kalvius, H. Karzel, W. Schiessl, M. Steiner, and M. Köfferlein, Phys. Rev. B **48**, 16 449 (1993).
[17] A. Svane and E. Antonçik, Phys. Rev. B **33**, 7462 (1986).
[18] J. E. Jaffe, R. Pandey, and A. B. Kunz, Phys. Rev. B **43**, 14 030 (1991).
[19] W. Potzel, in *Mössbauer Spectroscopy Applied to Magnetism and Materials Science*, edited by G. J. Long and P. Grandjean (Plenum, New York, 1993), Vol. 1, p. 305.
[20] W. Potzel, W. Adlassnig, J. Moser, C. Schäfer, M. Steiner, and G. M. Kalvius, Phys. Rev. B **39**, 8236 (1989).
[21] W. Adlassnig, W. Potzel, J. Moser, C. Schäfer, M. Steiner, and G. M. Kalvius, Nucl. Instrum. Methods Phys. Res. Sect. A **277**, 485 (1989) and references therein.
[22] To obtain quasihydrostatic conditions for a ^{67}ZnO sample proved to be uncritical: We have also tried paraffin and we have performed experiments without any pressure transmitting medium at all. The superconducting transition of the lead pressure gauge showed hardly any difference.
[23] U. Buchmann, Diploma thesis, Technische Universität Braunschweig, 1985.
[24] A. Eiling and J. S. Schilling, J. Phys. F **11**, 623 (1981).
[25] C. Schäfer, W. Potzel, W. Adlassnig, P. Pöttig, E. Ikonen, and G. M. Kalvius, Phys. Rev. B **37**, 7247 (1988).
[26] W. Potzel, Th. Obenhuber, A. Forster, and G. M. Kalvius, Hyperfine Interact. **12**, 135 (1982).
[27] W. Potzel and N. Halder, Nucl. Instrum. Methods Phys. Res. **226**, 418 (1984).
[28] A. Forster, W. Potzel, and G. M. Kalvius, Z. Phys. B **37**, 209 (1980).
[29] W. Potzel, High Pressure Res. **2**, 367 (1990).
[30] H. Karzel, U. Potzel, W. Potzel, J. Moser, C. Schäfer, M. Steiner, M. Peter, A. Kratzer, and G. M. Kalvius, Mater. Sci. Forum **79-82**, 419 (1991).
[31] E. F. Skelton, A. W. Webb, S. B. Qadri, S. A. Wolf, R. C. Lacoe, J. L. Feldman, W. T. Elam. E. R. Carpenter, Jr., and C. Y. Huang, Rev. Sci. Instrum. **55**, 849 (1984).
[32] I. L. Spain, E. F. Skelton, and F. Rachford, in *High Pressure Science and Technology*, edited by B. Vodar and P. Marteau (Pergamon, New York, 1979), p. 150.
[33] G. Huber, K. Syassen, and W. B. Holzapfel, Phys. Rev. B **15**, 5123 (1977).
[34] H. K. Mao, P. M. Bell, J. Shanen, and D. Steinberg, J. Appl. Phys. **49**, 3276 (1978).
[35] S. C. Yu, I. L. Spain, and E. F. Skelton, Solid State Commun. **25**, 49 (1978).
[36] A. Ohtani, M. Motobayashi, and A. Onodera, Phys. Lett. **75A**, 435 (1980).
[37] F. Birch, Phys. Rev. **71**, 809 (1947).
[38] M. Köfferlein, W. Potzel, M. Steiner, H. Karzel, W. Schiessl, and G. M. Kalvius, Phys. Rev. B **52**, 13 332 (1995).
[39] D. N. Talwar, M. Vandevyver, K. Kunc, and M. Zigone, Phys. Rev. B **24**, 741 (1981).
[40] B. A. Weinstein, Solid State Commun. **24**, 595 (1977).
[41] K. Thoma, B. Dorner, G. Duesing, and W. Wegener, Solid State Commun. **15**, 1111 (1974).
[42] M. Köfferlein, Diploma thesis, Physik-Department E15, Technische Universität München, 1993.
[43] D. W. Mitchell, Ph.D. thesis, State University of New York at Albany, 1993.
[44] P. Blaha, K. Schwarz, and R. Augustyn, Computer Code WIEN93, Technical University Vienna, 1993 [an improved and updated Unix version of the original copyrighted WIEN code, which was published by P. Blaha, K. Schwarz, P. Sorantin, and S. B. Trickey, Comput. Phys. Commun. **59**, 399 (1990)].
[45] P. Blaha, K. Schwarz, and P. H. Dederichs, Phys. Rev. B **37**, 2792 (1988).
[46] P. Blaha, K. Schwarz, and P. Herzig, Phys. Rev. Lett. **54**, 1192 (1985).
[47] P. Blaha, D. Singh, P. Sorantin, and K. Schwarz, Phys. Rev. B **46**, 1321 (1992).
[48] J. C. Phillips, *Bonds and Bands in Semiconductors* (Academic, New York, 1973).
[49] J. A. Majewski and P. Vogl, Phys. Rev. Lett. **57**, 1366 (1986); Acta Phys. Polonica A **73**, 341 (1988).
[50] K. Kunc and R. M. Martin, in *Ab Initio Calculations of Phonon Spectra*, edited by J. T. Devreese, V. E. Van Doren, and P. E. Van Camp (Plenum, New York, 1983), p. 65.
[51] W. Adlassnig, W. Potzel, J. Moser, C. Schäfer, M. Steiner, W. Schiessl, U. Potzel, M. Peter, and G. M. Kalvius, Hyperfine Interact. **54**, 759 (1990).
[52] W. Potzel, in *Condensed Matter Studies by Nuclear Methods*, edited by E. A. Görlich and K. Tomala (Stabill, Krakow, 1993), p. 116.
[53] W. Potzel, C. Schäfer, M. Steiner, H. Karzel, W. Schiessl, M. Peter, and G. M. Kalvius, Hyperfine Interact. **72**, 197 (1992).
[54] O. Madelung, W. von der Osten, and U. Rössler, in *Intrinsic Properties of Group IV Elements and III-V, II-VI, and I-VII Compounds*, edited by O. Madelung, Landolt-Börnstein, New Series, Group III, Vol. 22a (Springer, Berlin, 1987).
[55] S. Ves, K. Strössner, N. E. Christensen, C. K. Kimm, and M. Cardona, Solid State Commun. **56**, 479 (1985).
[56] W. Andreoni and K. Maschke, Phys. Rev. B **22**, 4816 (1980).
[57] G. J. Piermarini and S. Block, Rev. Sci. Instrum. **46**, 973 (1975).
[58] J. Albertsson, S. C. Abrahams, and Å. Kvick, Acta Crystallogr. B **45**, 34 (1989).